Catalysis Today 180 (2012) 117–123

Contents lists available at ScienceDirect

Catalysis Today

journal homepage: www.elsevier.com/locate/cattod

Solid state reactions in highly dispersed single and mixed lanthanide oxide–SiO_2 systems

Małgorzata A. Małecka*, Leszek Kępiński

Institute of Low Temperature and Structure Research, Polish Academy of Sciences, P.O. Box 1410, 50-950 Wrocław 2, Poland

ARTICLE INFO

Article history:
Received 17 December 2010
Received in revised form 15 February 2011
Accepted 6 March 2011
Available online 9 April 2011

Keywords:
Ceria based oxide
Ce–Yb–O
Nanostructured materials
Solid state reactions
Microstructure
Transmission electron microscopy (TEM)
Mixed oxide
Ytterbium silicate
$Yb_4[Si_3O_{10}][SiO_4]$

ABSTRACT

This paper summarizes our previous studies on the interaction of highly dispersed lanthanide oxides (La, Ce, Pr, Nd and Lu) with amorphous silica and presents new data on the $Ce_{0.5}Yb_{0.5}O_{1.75}$–SiO_2 system. It is shown that at temperatures above 800 °C, chemical reaction between lanthanide oxide and silica may occur leading to formation of silicate phases with unusual structure not observed for bulk like oxide–SiO_2 systems. For nano $Ce_{0.5}Yb_{0.5}O_{1.75}$–SiO_2 system results of TEM, SEM and XRD studies revealed that at or above 1000 °C, ytterbium is withdrawn from the mixed oxide and B-type polymorph of $Yb_2Si_2O_7$ ($Yb_4[Si_3O_{10}][SiO_4]$) is formed. This polymorph, till now known as high pressure form, is unstable at 1100 °C and transforms into ordinary C-type $Yb_2Si_2O_7$. Mechanism of silicate formation and its possible role in deactivation of supported catalysts containing lanthanide oxides as active phase or as promoters is discussed.

1. Introduction

Highly dispersed lanthanide oxides play important role in various fields of modern technology. In catalysis they are often used as active components or as promoters, as for example in alumina supported noble metal catalysts used as three way converters of car exhaust gas. In such systems one of lanthanide dopant roles is stabilization of γ-Al_2O_3 support against sintering and hindering a phase transformation into α-Al_2O_3 (corundum). Mechanism of the stabilization involves strong interaction of lanthanide ions with alumina surface with formation of a surface compound [1]. Relatively less is known on the interaction of lanthanide oxides with the silica support, though such systems were studied as catalysts active e.g. in alpha-pinene isomerization (La, Pr, Sm, Eu, Tb, and Yb) [2] or in TWC process (Pd/CeO_2–SiO_2) [3].

Existing literature shows that at elevated temperatures solid state reaction between lanthanide oxide and high area silica occurs with formation of silicates. This process drastically changes the microstructure of the system and clearly influences the catalytic activity of lanthanide ions (e.g. as reversible change of the oxidation state) [4,5]. Analysis of lanthanide oxide–SiO_2 binary diagrams reveals that silicates with various stoichiometry can be formed: Ln_2SiO_5 (Ln_2O_3:SiO_2 = 1:1), $Ln_{9.33}Si_6O_{26}$ (7:9) and $Ln_2Si_2O_7$ (1:2) [6–8]. Moreover, extensive polymorphism of $Ln_2Si_2O_7$ occurs, with nine polymorphic forms (A, B, C, D, E, F, G, H, I) observed depending on lanthanide ion radius and temperature [6,9–11]. Below 1500 °C at normal pressure, A-, B- and C-type of structures are typical for light, medium and heavy lanthanide ions, respectively, while at higher temperatures D-, E-, F- or G-types are stable [6,9]. Under high pressure conditions, new structures called X, K and L have been found [12–14].

Recent studies on highly dispersed lanthanide oxides deposited on high surface SiO_2 revealed that surface silicates with unexpected I- and B-type structure form for La [15], Pr [5], Nd [16] and Lu [4] at low temperature (<1100 °C). Both I and B-type are not "real" disilicates, because they do not have $[Si_2O_7]^{-6}$ groups in the structure. Their correct structure formula are: $Ln_6[Si_4O_{13}][SiO_4]_2$ for I-type (observed for La–Nd) and $Ln_4[Si_3O_{10}][SiO_4]$ for B-type (observed for heavy lanthanides). At higher temperatures I- and B-type of silicates transform into usual A- and C-type, respectively.

To our best knowledge there is no data in the literature on the interaction of mixed lanthanide oxides with high surface silica. There are however, few works devoted to mixed lanthanide oxides $Ce_{1-x}Tb_xO_{2-y}$, [17,18] or $Ce_{1-x}Pr_xO_{2-y}$ [19,20] on alumina or La modified alumina. It has been found that stability of nanocrystalline mixed oxides (4–16 nm) supported on alumina

* Corresponding author. Tel.: +48 71 3435021; fax: +4871 441029.
E-mail address: M.Malecka@int.pan.wroc.pl (M.A. Małecka).

0920-5861/$ – see front matter © 2011 Elsevier B.V. All rights reserved.
doi:10.1016/j.cattod.2011.03.022

depends on temperature and atmosphere of thermal treatment. In reducing atmosphere, perovskite phase $LnAlO_3$ (Ln = Ce, Pr or Tb) was observed after heating at 900 °C [17,19,20]. In contrast, $Ce_{0.8}Tb_{0.2}O_{2-y}$ mixed oxide supported on modified alumina surface appeared to be stable at temperature up to 900 °C in oxidizing and inert atmosphere [17,18].

In this work, the microstructure and thermal stability of a new $Ce_{0.5}Yb_{0.5}O_{1.75}$–SiO_2 system, was studied at temperatures up to 1100 °C in air. The main goal was observation of possible chemical reactions between nanocrystalline mixed oxide and silica support that could lead to segregation of the oxide components and formation of surface silicates. Samples subjected to various treatments were thoroughly characterized by XRD, TEM, SEM–EDS and FTIR. Results obtained are compared with earlier data on structural stability of single LnO_x–SiO_2 systems (Ln = La, Ce, Pr, Nd, Lu).

2. Materials and methods

LnO_x–SiO_2 samples were prepared by impregnation of a high surface silica with an aqueous solution of lanthanide nitrate (La, Nd, Yb and Lu) [4,15,16] or with a suspension of nanooxide (CeO_2, PrO_x, $Ce_{0.5}Yb_{0.5}O_{1.75}$). 20 wt% colloidal suspension of CeO_2 (Aldrich Product No. 28.924-4) or a suspension of an amorphous PrO_x oxide precursor in methanol was used [5,21]. $Ce_{0.5}Yb_{0.5}O_{1.75}$–SiO_2 samples were synthesized as follows. First nanoparticles of $Ce_{0.5}Yb_{0.5}O_{1.75}$ were by prepared by W/O (water-in-oil) microemulsion method [5]. Then, as-prepared, dense suspension of the oxide in organic phase was washed several times with distilled water to remove the surfactant. Finally, small amount of acetic acid (to pH = ~4) was added to create a stable dispersion. High surface silica (Degussa OX-130, $S_0 = 170\ m^2/g$) was impregnated with the dispersion to get $Ce_{0.5}Yb_{0.5}O_{1.75}$–SiO_2 sample with a molar ratio SiO_2:$Ce_{0.5}Yb_{0.5}O_{1.75}$ = 14:1. After drying at 120 °C overnight, the sample was pre-heated at 550 °C for 3 h in oxygen flow to clean out organic residues and remaining nitrate groups. Such standardized sample (called "as-prepared") was heated at temperatures from 800 to 1100 °C in static air.

Phase composition and lattice parameter of the samples were determined by XRD (PANalitical X'Pert PRO X-ray powder diffractometer, Cu K_α radiation) with FullProf program [22] used for display and analysis of the diffractograms. Morphology and microstructure was investigated by TEM (Philips CM-20 SuperTwin operating at 200 kV and providing 0.25 nm resolution). HRTEM images and SAED patterns were analysed with DigitalMicrograph program. JEMS program was used for simulation of HRTEM images. Uniformity and chemical composition of the samples was checked with FE-SEM microscope (FEI NovaNanoSEM 230) equipped with EDS analyzer (EDAX Genesis XM4).

3. Results and discussion

3.1. Single lanthanide oxide–silica

Morphology and phase evolution of highly dispersed LnO_x–SiO_2 systems upon thermal treatment has been described in our previous papers for La [15], Ce [21], Pr [5], Nd [16] and Lu [4]. Morphology of the as-prepared samples (i.e., after pretreatment in air at 550 °C) was closely related to the synthesis procedure. Well-defined crystalline particles of CeO_2 [21] or Pr_6O_{11} [5] with mean size of ca. 5 nm were present in the samples obtained by impregnation of SiO_2 with suspension of oxide nanoparticles. In contrast, no distinct lanthanide oxide phase was formed in the samples prepared by impregnation of the support with an aqueous solution of La- [15] and Nd- [16] nitrates. Instead formation of a nanometer thick amorphous layer of $Ln_xSi_yO_z$ silicate on the silica surface was observed. For silica impregnated with Lu nitrate both amorphous silicate and nanocrystalline Lu_2O_3 were observed [4]. In this case, however, high surface coverage of silica with lanthanide was used, resulting probably in formation of three dimensional aggregates of nitrate not in direct contact with silica surface.

As the result of heat treatment decrease of the surface area of Ln_2O_3–silica systems was observed. For La_2O_3–SiO_2 obtained by impregnation of high surface SiO_2 (Degussa OX-130) with an aqueous solution of La nitrate the BET surface area (calculated per gram of the support) decreased from 150 m^2/g at 600 °C to 60 m^2/g at 1100 °C. Up to 950 °C only slight (~30 m^2/g) decrease but then at 1000 °C rapid loss of the surface area occurred. This behavior reflected generally the loss of surface area of the bare silica support: decrease from 170 to 160 m^2/g between 600 and 950 °C and then surface loss to 119 and 71 m^2/g at 1000 and 1100 °C, respectively [15].

Annealing of nanocrystalline CeO_2 supported on SiO_2 in oxidizing atmosphere at temperatures up to 1100 °C, caused only crystallite growth of CeO_2 and sintering of the silica support [21]. CeO_2 crystals often assumed spherical shape, probably to minimize CeO_2–SiO_2 interface. No solid state reaction between ceria and silica was detected, presumably because Ce^{4+} ions cannot be reduced under such conditions to Ce^{3+} ions found in all known Ce silicates [23]. An exception is $CeSiO_4$ that however, forms only at hydrothermal conditions [24]. In accordance with this fact, formation of various Ce silicates was observed for CeO_2–SiO_2 systems heated in reducing atmosphere [25–27]. In literature, absence of CeO_2–SiO_2 reaction in oxidizing atmosphere up to 1200 °C was also reported in [28–31], whereas cerium silicates were observed in reducing atmosphere [32,33].

Different behavior was found for Pr_6O_{11} nanocrystals deposited on silica surface [5]. Already after heating at 800 °C in air, partial amorphization and spreading of the oxide was observed by XRD and HRTEM. At 950 °C an amorphous praseodymium silicate formed, which then at 1000 °C crystallized into unusual I type $Pr_2Si_2O_7$. For LnO_x–SiO_2 prepared by impregnation I-type silicates crystallized already at 950 °C for La [15] and Nd [16]. In line with our results, formation of an amorphous Ln-silicate at 800–900 °C, with no intermediate Ln oxide phase was reported for high surface silica impregnated with La, Pr Sm, Eu, Tb, and Yb nitrates [2,34,35]. Amorphous or poorly ordered lanthanide silicates were also observed below 1000 °C in LnO_x–SiO_2 systems prepared by sol–gel, deposition–precipitation or vacuum evaporation [36–38].

After treatment at 1000 °C or higher, crystalline lanthanide silicates of various structure were observed in all LnO_x–SiO_2 systems studied by us, regardless of preparation method (Table 1). For light Ln^{3+}-ions (La, Pr, Nd) [5,15,16], I-type $Ln_2Si_2O_7$ silicates (proper formula $Ln_6[Si_4O_{13}][SiO_4]_2$) occurred at the lowest temperature. Then, with increasing temperature, this phase transformed into A-type $Ln_2Si_2O_7$ (structure formula $Ln_2[Si_2O_7]$). For heavy Ln^{3+}-ions (Yb, Lu) [4, this work] B-type silicate (proper formula $Lu_4[Si_3O_{10}][SiO_4]$) occurred as the first crystalline phase which, at higher temperatures, transformed into C-type structure (structure formula $Ln_2[Si_2O_7]$).

Formation of oligosilicates $Ln_6[Si_4O_{13}][SiO_4]_2$ (I-type) and $Ln_4[Si_3O_{10}][SiO_4]$ (B-type) for light (La, Pr, Nd) and heavy (Lu, Yb) lanthanides at temperatures between 1000 °C and 1100 °C was unexpected in view of classic phase diagram presented by Felsche [9] (Fig. 1). However, other authors also reported that under special conditions such oligosilicates may occur for La [11], Lu, Yb and Tm [12,39].

3.2. Mixed lanthanide oxide–silica

EDX analysis of a dried dispersion of $Ce_{0.5}Yb_{0.5}O_{1.75}$ nanoparticles used for preparation of the mixed oxide–silica

Table 1
Crystalline silicate phases identified in various LnO_x–SiO_2 samples heated in air.

Temp.	La (Imp)[a] [15]	Ce (NP)[a][21]	Pr (NP) [5]	Nd (Imp) [16]	Lu (Imp) [4]	$Ce_{0.50}Yb_{0.50}$ (NP)[this work]
950 °C	I	Oxide	I	I	Oxide	Oxide
1000 °C	I	Oxide	I	I	B	B
1100 °C	I	Oxide	I or/and A	I	B	B or/and C
1200 °C	A	Oxide	–	A	C	–

[a] Sample prepared by impregnation with aqueous solution of Ln nitrate or with dispersion of nanoparticles, respectively.

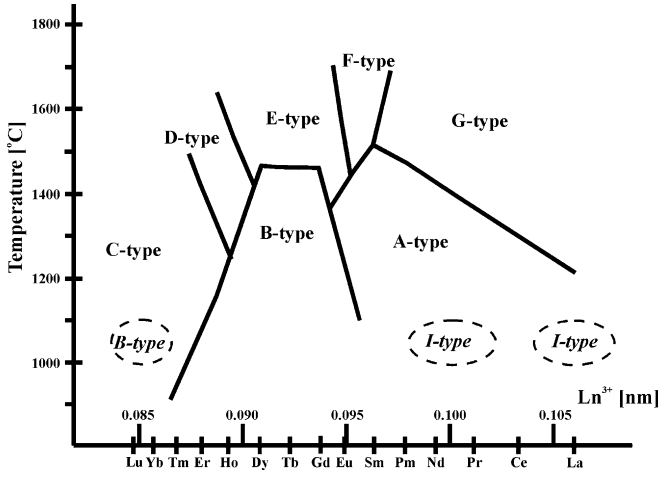

Fig. 1. Stability range of silica rich lanthanide silicates ($Ln_2O_3 + 2SiO_2$) according to [9]. New I- and B-type structures obtained at low temperatures are included.

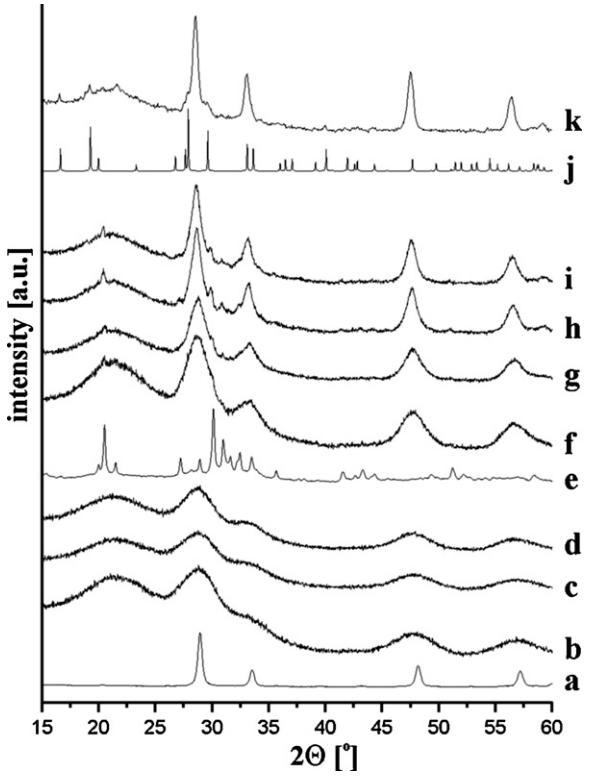

Fig. 3. XRD diffractograms of $Ce_{0.50}Yb_{0.50}O_{1.75}$–$SiO_2$ sample subjected to various heat treatment. (a) Unsupported $Ce_{0.50}Yb_{0.50}O_{1.75}$, (b) 550 °C/3 h O_2, (c) 800 °C/3 h air, (d) 900 °C/3 h air, (e) B-type $Yb_2Si_2O_7$ standard, (f) 1000 °C/3 h air, (g) 1040 °C/3 h air, (h) 1080 °C/3 h air, (i) 1100 °C/3 h air, (j) C-type $Yb_2Si_2O_7$ standard, (k) 1100 °C/28 h air.

sample confirmed an assumed chemical composition of the oxide (Ce/Yb = 1/1). Fig. 2 shows TEM and HRTEM images of $Ce_{0.50}Yb_{0.50}O_{1.75}$–$SiO_2$ after pre-treatment at 550 °C for 3 h in oxygen flow. It is seen that the mixed oxide is homogeneously distributed on SiO_2 surface as individual crystallites or small clusters of crystallites. Particle size distribution measured form TEM micrographs (inset to Fig. 2) is relatively narrow with mean particle size of 2.2 nm. Lattice fringes with 0.32 nm spacing seen on the particles, correspond to $(2\,2\,2)_C$ planes of $Ce_{0.50}Yb_{0.50}O_{1.75}$ with C#-type (defected C-type) cubic structure. This observation was confirmed by XRD pattern (Fig. 3b), where wide reflections at positions expected for $Ce_{0.50}Yb_{0.50}O_{1.75}$ together with very broad signal (~20°) of amorphous silica occurred. Generally, morphology of the sample resembled that seen for CeO_2 and Pr_6O_{11} nanoparticles supported on silica [5,21]. Thermal stability of the "as prepared" sample was then studied by observation of structure change upon heat

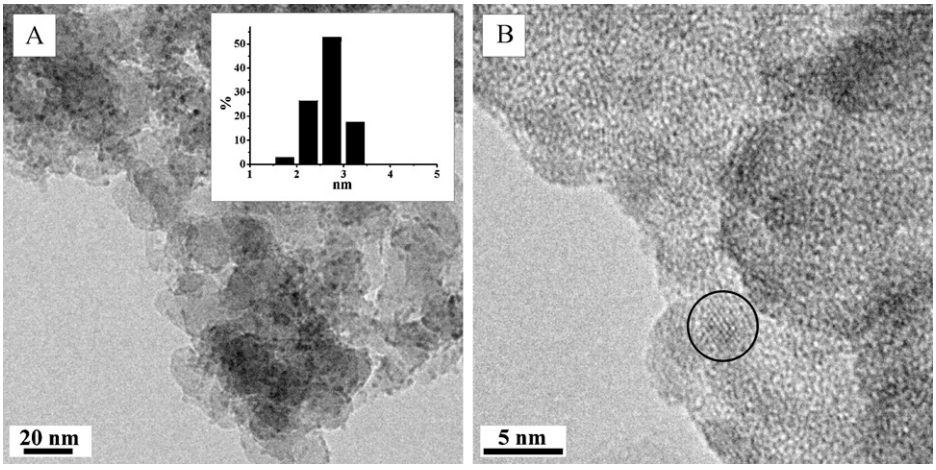

Fig. 2. TEM (A) and HRTEM (B) images of $Ce_{0.50}Yb_{0.50}O_{1.75}$–$SiO_2$ sample after heating at 550 °C for 3 h in O_2. Crystallite size distribution is included as inset to A.

treatment at 800, 900, 1000, 1020, 1040, 1060, 1080 and 1100 °C in static air. Results of the XRD and HRTEM experiments are summarized in Table 2.

Both XRD and TEM revealed high structure stability of the mixed oxide on silica up to 900 °C. In XRD diffractograms (Fig. 3 trace c and d) hardly any change can be seen in widths and positions of the reflections. Lattice parameter of $Ce_{0.50}Yb_{0.50}O_{1.75}$ determined from traces b, c and d was $a_F = 1/2\ a_C = \sim 0.535$ nm and mean crystallite size was ~2 nm. TEM and SAED images of the $Ce_{0.50}Yb_{0.50}O_{1.75}$–$SiO_2$ sample after heating at 800 °C are shown in Fig. 4. In the SAED pattern obtained from a large area rings visible at d = 0.32, 0.27, 0.23, 0.19, 0.16 and very weak 0.44 nm, correspond to $(2\,2\,2)_C$, $(4\,0\,0)_C$, $(3\,3\,2)_C$, $(4\,4\,0)_C$, $(6\,2\,2)_C$ and $(2\,1\,1)_C$ planes of $Ce_{0.50}Yb_{0.50}O_{1.75}$ (cubic C#-type structure), respectively. This result agrees with our earlier study on unsupported Yb-doped ceria, where it was shown that depending on composition the structure of the oxide can be described as defected cubic F or C-type [40]. In HRTEM micrographs (e.g. Fig. 4B) $Ce_{0.50}Yb_{0.50}O_{1.75}$ crystallites could be identified as areas exhibiting 0.32 nm lattice fringes corresponding to $(2\,2\,2)_C$ planes. Mean crystallite size determined from HRTEM (3.5 nm) was higher than that measured from XRD (2.2 nm). The difference could be due to large lattice strain contribution to the peaks broadening in XRD.

The first signs of a solid state reaction between the mixed oxide and the silica occurred in the sample heated at 1000 °C for 3 h. In XRD pattern of this sample (Fig. 3f) very weak peak, characteristic for triclinic of $Yb_2Si_2O_7$ (PDF File nr. 00-030-1439), appeared at 20.4°. Intensity of the peaks characteristic for this silicate enhanced with increasing temperature up to 1100 °C. The triclinic $Yb_2Si_2O_7$ appears to be isostructural with B-type Tm and Lu silicates [4,39,41], but till now was observed only at high pressure [39]. In order to explain this inconsistency we tried to synthesize B-type $Yb_2Si_2O_7$ at normal pressure by thermal treatment of a high surface silica impregnated with Yb nitrate, according to the procedure used previously for Lu [4]. Fig. 5A (red dots) shows XRD pattern of the sample heated at 1000 °C for 3 h, together with the result of structure refinement performed with FullProf [22]. As a starting mode for the refinement the structure of B-$Tm_2Si_2O_7$ was used [41]. Due to complex background caused by the presence of an amorphous phase accuracy of the refinement was not good enough to enable determination of all atomic parameters. It appears, however that there is reasonable fit between experimental and calculated patterns, what proves that the structure model applied was correct. Unit cell parameters refined for the silicate are given in Table 3. Further evidence for the presence of B-type $Yb_2Si_2O_7$ has been obtained from FTIR spectrum (Fig. 5B), which contains bands at 693 and 723 cm^{-1}, characteristic for $[Si_3O_{10}]$ groups [4]. Above results indicate that under normal pressure conditions, used to in this work, B-type $Yb_2Si_2O_7$ may form also in $Ce_{0.50}Yb_{0.50}O_{1.75}$–$SiO_2$ system. Unit cell parameters measured for the sample heated at 1100 °C are similar to those measured for the impregnated sample (Table 3). Fig. 6 shows HRTEM image, with corresponding FFT pattern, of B-type $Yb_2Si_2O_7$ crystal in [00–1] orientation found in the $Ce_{0.50}Yb_{0.50}O_{1.75}$–$SiO_2$ heated at 1080 °C. Good correspondence between the observed HRTEM image and that simulated using the crystal structure determined by Rietveld refinement (inset to Fig. 6) also validates the proposed structure of the silicate.

Prolonged heating of $Ce_{0.50}Yb_{0.50}O_{1.75}$–$SiO_2$ at 1100 °C (28 h) caused gradual decline of the reflections of B-type $Yb_2Si_2O_7$ in XRD pattern and simultaneous appearance of reflections of monoclinic Cftype $Yb_2Si_2O_7$ (Fig. 3k), which is considered as thermodynamically stable polymorph at normal pressure and at low temperatures [9,12].

It is interesting to compare the behavior of the $Ce_{0.50}Yb_{0.50}O_{1.75}$–$SiO_2$ with that of Yb_2O_3 supported on silica. Yamamoto et al., in a series of papers [2,42,43], studied thoroughly

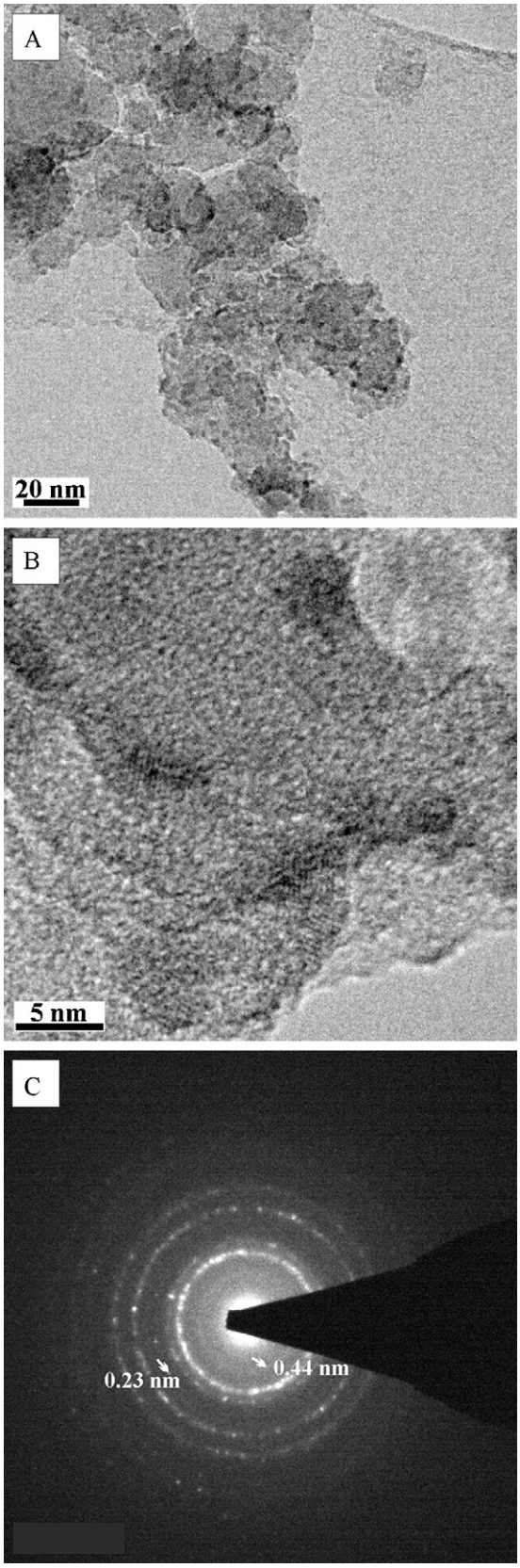

Fig. 4. TEM (A), HRTEM (B) images and SAED pattern (C) of $Ce_{0.50}Yb_{0.50}O_{1.75}$–$SiO_2$ sample heated at 800 °C for 3 h in air.

Table 2
Characterization of $Ce_{0.50}Yb_{0.50}O_{1.75}$–$SiO_2$ sample subjected to various treatments.

Treatment	Phases present	x	Lattice parameter (a_F) [nm]	Mean crystallite size	
				XRD [nm]	TEM [nm]
550 °C/3 h O_2	SiO_2 (a) $Ce_{1-x}Yb_xO_{2-(x/2)}$ (c)	0.5(0.5)[a]	0.5352(0.5360)[a]	2.2(5.0)[a]	2.7[2–4]
800 °C/3 h air	SiO_2 (a) $Ce_{1-x}Yb_xO_{2-(x/2)}$ (c)	0.5(0.5)[a]	0.5345(0.5351)[a]	1.9(12.9)[a]	4.1[2–10]
900 °C/3 h air	SiO_2 (a) $Ce_{1-x}Yb_xO_{2-(x/2)}$ (c)	0.45(0.5)[a]	0.5362(0.5345)[a]	2.2(21.7)[a]	3.5[2–9]
1000 °C/3 h air	SiO_2 (a) $Ce_{1-x}Yb_xO_{2-(x/2)}$ (c) $Yb_2Si_2O_7$ (B)	0.3	0.5379	3.2	3.9[2–9]
1020 °C/3 h air	SiO_2 (a) $Ce_{1-x}Yb_xO_{2-(x/2)}$ (c) $Yb_2Si_2O_7$ (B)	0.25	0.5384	3.6	4.6[2–24]
1040 °C/3 h air	SiO_2 (a) $Ce_{1-x}Yb_xO_{2-(x/2)}$ (c) $Yb_2Si_2O_7$ (B)	0.2	0.5396	4.2	5.6[2–19]
1060 °C/3 h air	SiO_2 (a) $Ce_{1-x}Yb_xO_{2-(x/2)}$ (c) $Yb_2Si_2O_7$ (B)	0.15	0.5398	5.3	7[3–14]
1080 °C/3 h air	SiO_2 (a) $Ce_{1-x}Yb_xO_{2-(x/2)}$ (c) $Yb_2Si_2O_7$ (B)	0.1	0.5400	6.2	7.3[3–26]
1100 °C/3 h air	SiO_2 (a) $Ce_{1-x}Yb_xO_{2-(x/2)}$ (c) $Yb_2Si_2O_7$ (B)	0.1	0.5401	7.2	8.8[3–20]
1100 °C/28 h air	SiO_2 (a) $Ce_{1-x}Yb_xO_{2-(x/2)}$ (c) $Yb_2Si_2O_7$ (B + C)	~0(0.5)[a]	0.5405(0.5343)[a]	12.3(53.4)[a]	–

a – amorphous; c – cubic structure; B – B-type of $Yb_2Si_2O_7$ (triclinic structure); C – C-type of $Yb_2Si_2O_7$ (monoclinic structure).
[a] Results obtained for unsupported $Ce_{0.50}Yb_{0.50}O_{1.75}$ mixed oxide after similar treatment [40].

the Yb_2O_3/SiO_2 catalysts obtained by impregnation of a high surface SiO_2 with an aqueous solution of Yb nitrate over wide range of Yb loadings up to 62 wt% Yb_2O_3. Basing on experimental data obtained with various methods (including XRD, EXAFS, Raman, BET and various chemical techniques) the authors claimed that up to the highest loading and calcination temperature up to 800 °C no crystalline phases were observed and Yb existed at the surface as individual YbO_6 octahedra strongly interacting with the silica surface. After calcination at 1000 °C, Raman spectra showed the appearance of new bands that the authors assigned to unidentified Yb silicate [2]. For $Ce_{0.50}Yb_{0.50}O_{1.75}$–$SiO_2$ formation of crystalline Yb silicate was also detected after heating at 1000 °C and we proved that the silicate is B-type polymorph of $Yb_2Si_2O_7$ reported in the literature as high pressure form [12,39]. The question is why, in contrast to the present observation, B-type $Yb_2Si_2O_7$ was previously observed only at high pressure and high temperature? In previous work [4], we showed that in similar highly dispersed Lu_2O_3–SiO_2 system the B-type $Lu_2Si_2O_7$ ($Lu_4[Si_3O_{10}][SiO_4]$) occurred after heating at 1000 °C and we presented arguments that this is in fact a preferred low temperature structure for all heavy lanthanides. However, due to kinetic limitations at low temperature, this polymorph cannot be obtained by classic ceramic route, i.e. direct solid state reaction between macroscopic, crystalline Ln_2O_3 (Ln = Tm, Yb and Lu) and SiO_2. Very high dispersion of lanthanide over the high surface amorphous silica obtained via impregnation with nitrate solution or nanoparticle dispersion enables the intimate lanthanide–silica contact and decreases the reaction barrier.

Formation of ytterbium silicate as the result of a solid state reaction between $Ce_{0.50}Yb_{0.50}O_{1.75}$ and SiO_2 requires a transfer of Yb^{3+}-ions from the mixed oxide to the support. The depletion of the mixed oxide in Yb^{3+}-ions manifested itself in XRD patterns as a shift the oxide reflections towards lower angles caused by continuous growth of the cell parameter from $a_F = 1/2\ a_C = 0.5352$ nm (corresponding to $Ce_{0.5}Yb_{0.5}O_{1.75}$ [40]) to $a_F = 0.5405$ nm (close to pure ceria) with increasing calcination temperature (Fig. 3). It is seen that in accordance with the proposed mechanism of Yb silicate formation in $Ce_{0.50}Yb_{0.50}O_{1.75}$–$SiO_2$ the amount of this phase formed at 1000 °C is very small, much smaller than in Yb_2O_3–SiO_2 sample subjected to identical heat treatment (cf. Figs. 3f and 5A). Morphology of particles of the mixed oxide strongly depleted in Yb differed dramatically from that of the silicate. In the samples heated above 1060 °C the oxide particles exhibited spherical shape with a mean size ~10 nm. Fig. 7 presents HRTEM image and microdiffraction pattern of such a particle in [1 1 0] orientation. The growth of spherical particles is correlated with severe sintering of the silica support above 1000 °C, which manifests itself as sudden decline of the specific surface area [15]. The spherical shape minimizes the

Table 3
Comparison of lattice parameters of B-type silicates (P -1 space group) identified in this work with literature data.

Sample	a [nm]	b [nm]	c [nm]	Alpha [°]	Beta [°]	Gamma [°]
$Ce_{0.50}Yb_{0.50}O_{1.75}$–$SiO_2$ 1080 °C	0.656	0.663	1.201	94.01	91.58	92.01
Yb_2O_3–SiO_2 1000 °C	0.6530	0.6581	1.1915	94.36	91.28	92.09
$Yb_2Si_2O_7$ PDF Card 00-030-1439	0.6530	0.6550	1.1890	94.28	91.15	91.75
B-type $Tm_2Si_2O_7$ PDF Card 00-031-1391	0.6548	0.6576	1.1920	94.39	91.19	91.81

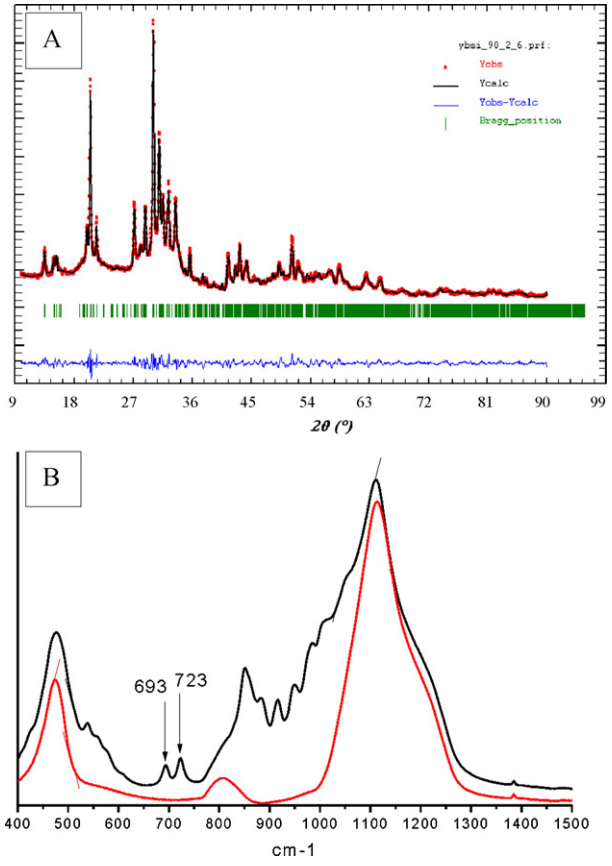

Fig. 5. Refinement of the structure of B-type $Yb_2Si_2O_7$ formed in Yb_2O_3–SiO_2 sample heated at 1000 °C for 3 h (A) and FTIR spectra of the sample (B).

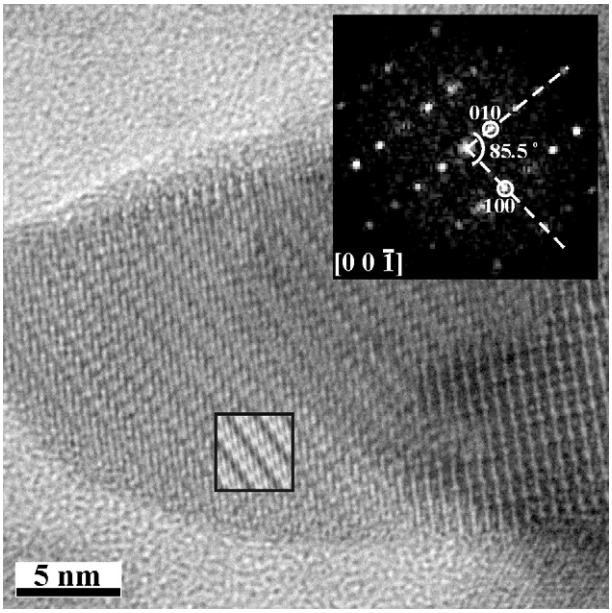

Fig. 6. HRTEM image, with corresponding FFT pattern, of B-type $Yb_2Si_2O_7$ crystallite. Simulated image is included as inset.

interface surface area between the oxide particles and surrounding silica matrix. Overall morphology of the $Ce_{0.50}Yb_{0.50}O_{1.75}$–$SiO_2$ sample heated at high temperatures is presented in SEM image (Fig. 8). The image, formed using back-scattered electrons (material contrast), shows both spherical particles of the oxide and irregular silicate crystallites uniformly distributed within the silica grains.

A positive effect of silica support on the structure stability of $Ce_{0.50}Yb_{0.50}O_{1.75}$ nanocrystals becomes apparent when results presented in this work are compared with those for the unsupported oxide [40]. As expected, sintering of the supported particles has been strongly restricted with hardly any growth of a mean crystallite size up to 900 °C (Table 2). Under the same conditions mean crystallite size of the unsupported oxide increased four times. On the other hand, decomposition of the mixed oxide supported on silica was observed at or above 1000 °C due to formation of ytterbium silicate, whereas the unsupported mixed oxide showed no evidence of the phase separation even after very long (45 h) thermal treatment at 1100 °C [40]. It appears therefore, that high surface silica may be used as an inert support for nanocrystalline ceria doped with ytterbium (and possibly other lanthanides) only at temperatures up to 900 °C. At higher temperatures adverse effects (oxide decomposition due to formation of silicates and severe sintering of silica) probably preclude usage of silica as catalytic support. It should be mentioned also that in reducing atmosphere such adverse effects may occur at much lower temperatures (above 700 °C) due to possible formation of cerium silicates [25–27,32,33].

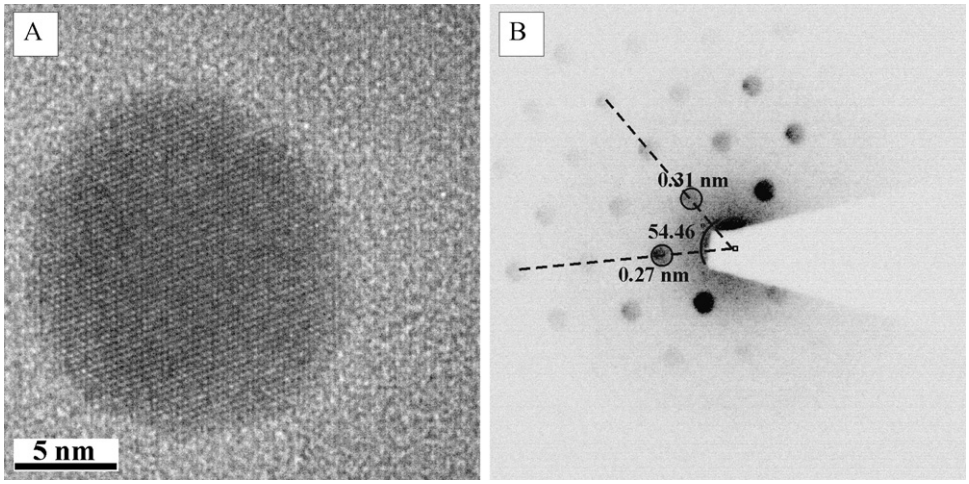

Fig. 7. HRTEM image (A) and microdiffraction pattern (B) of a spherical Yb depleted oxide particle in silica matrix.

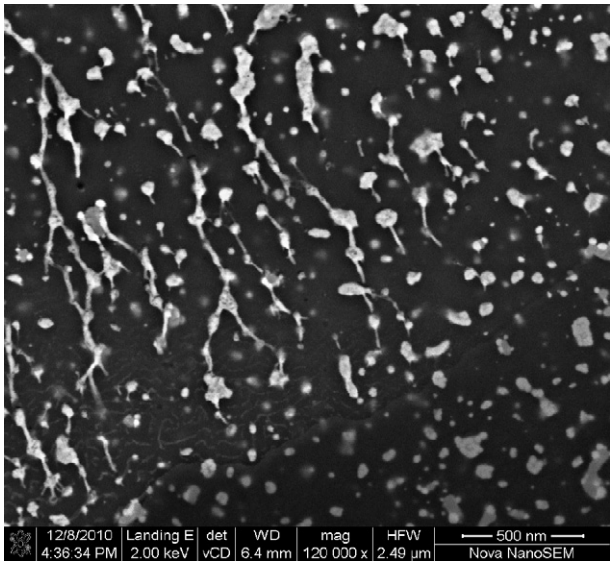

Fig. 8. SEM image of $Ce_{0.50}Yb_{0.50}O_{1.75}$–$SiO_2$ sample heated at 1100 °C for 28 h in air.

4. Conclusions

Nanocrystalline $Ce_{0.50}Yb_{0.50}O_{1.75}$ mixed oxide (~2 nm mean particle size) prepared by microemulsion method was uniformly distributed over the surface of high surface SiO_2 from an aqueous suspension.

The nano-sized $Ce_{0.50}Yb_{0.50}O_{1.75}$ supported on silica exhibited very high textural and structural stability in air up to 900 °C. At 1000 °C decomposition of the supported oxide was observed, due to migration of Yb^{3+}-ions to silica and formation of ytterbium silicate.

The ytterbium silicate formed at 1000 °C exhibited unusual, B-type $Yb_2Si_2O_7$ structure (proper formula $Yb_4[Si_3O_{10}][SiO_4]$), till now observed only at high pressure. At 1100 °C this silicate slowly transformed into monoclinic C-type $Yb_2Si_2O_7$.

High surface silica may be used as an inert support for nanocrystalline ceria doped with ytterbium (and possibly other lanthanides) in oxidizing atmosphere at temperatures up to 900 °C. At higher temperatures adverse effects (oxide decomposition due to formation of silicates and severe sintering of silica) occur. In reducing atmosphere such adverse effects may occur at much lower temperatures (above 700 °C) due to possible formation of cerium silicates.

Acknowledgments

This work is dedicated to Professor Serafin Bernal on the occasion of his 65th birthday.

The authors thank Mrs. Z. Mazurkiewicz for valuable help with preparation of the samples, Mrs. E. Bukowska for XRD and Mr. M. Ptak for FTIR work.

References

[1] S. Boullosa-Eiras, E. Vanhaecke, T. Zhao, D. Chen, A. Holmen, Catal. Today (2010) 038, doi:10.1016/j.cattod.2010.05.
[2] T. Yamamoto, T. Matsuyama, T. Tanaka, T. Funabiki, S. Yoshida, Phys. Chem. Chem. Phys. 1 (1999) 2841–2849.
[3] J.R. Gonzalez-Velasco, M.A. Gutierrez-Ortiz, J.A. Botas, S. Bernal, J.M. Gatica, J.A. Perez-Omil, Stud. Surf. Sci. Catal. 126 (1999) 187–189.
[4] L. Kępiński, M. Mączka, M. Drozd, J. Alloys Compd. 443 (2007) 132–142.
[5] M.A. Małecka, L. Kepiński, J. Alloys Compd. 430 (2007) 282–291.
[6] J. Felsche, Struct. Bond. 13 (1973) 99–197.
[7] J. Wang, S. Tian, G. Li, F. Liao, X. Jing, Mater. Res. Bull. 36 (2001) 1855–1861.
[8] M. Higuchi, Y. Masubuchi, S. Nakayama, S. Kikkawa, K. Kodaira, Solid State Ionics 174 (2004) 73–80.
[9] J. Felsche, J. Less-Comm. Met 2 (1970) 1–14.
[10] H. Muller-Bunz, T. Schleid, Z. Anorg. Allg. Chem. 626 (2000) 2549–2556.
[11] H. Muller-Bunz, T. Schleid, Z. Anorg. Allg. Chem. 628 (2002) 564–569.
[12] M.E. Fleet, X. Liu, J. Solid State Chem. 178 (2005) 3275–3283.
[13] M.E. Fleet, X. Liu, J. Solid State Chem. 161 (2001) 166–172.
[14] M.E. Fleet, X. Liu, Am. Miner. 89 (2–3) (2004) 396–404.
[15] L. Kępiński, W. Miśta, J. Okal, M. Drozd, M. Mączka, Solid State Sci. 7 (2005) 1300–1311.
[16] L. Kępiński, M. Wołcyrz, M. Drozd, Mater. Chem. Phys. 96 (2006) 353–360.
[17] S. Bernal, G. Blanco, G.A. Cifredo, J.J. Delgado, D. Finol, J.M. Gatica, J.M. Rodriguez-Izquierdo, H. Vidal, Chem. Mater. 14 (2002) 844–850.
[18] B.M. Reddy, P. Saikia, P. Bharali, S.-E. Park, M. Muhler, W. Gronert, J. Phys. Chem. C 113 (6) (2009) 2452–2462.
[19] M. Lopez-Haro, K. Aboussaid, J.C. Gonzalez, J.C. Hernandez, J.M. Pintado, G. Blanco, J.J. Calvino, P.A. Midgley, P. Bayle-Guillemaud, S. Trasobares, Chem. Mater. 21 (2009) 1035–1045.
[20] K. Aboussaid, S. Bernal, G. Blanco, G.A. Cifredo, A. Galtayries, J.M. Pintadoa, M.S. el Begranib, Surf. Interface Anal. 40 (2008) 250–253.
[21] L. Kępiński, D. Hreniak, W. Stręk, J. Alloys Compd. 341 (2002) 203–207.
[22] J. Rodriguez-Carvajal, Physica B 192 (1993) 55–69.
[23] M.S. Wickleder, Chem. Rev. 102 (2002) 2011–2087.
[24] J.M.S. Skakle, C.L. Dickson, F.P. Glasser, Powder Diffr. 15 (4) (2000) 234–238.
[25] L. Kepinski, M. Wolcyrz, Catal. Lett. 15 (1992) 329–337.
[26] L. Kepinski, M. Wolcyrz, J. Solid State Chem. 131 (1997) 121–130.
[27] L. Kepinski, M. Wolcyrz, M. Marchewka, J. Solid State Chem. 168 (2002) 110–118.
[28] B.M. Reddy, A. Khan, Catal. Surv. Asia 9 (3) (2005) 1155–1171.
[29] H. Cui, M. Zayat, D. Levy, J. Alloys Compd. 474 (2009) 292–296.
[30] H.A.M. van Hal, H.T. Hintzen, J. Alloys Compd. 179 (1992) 77–85.
[31] R. Craciun, Solid State Ionics 110 (1998) 83–93.
[32] E. Rocchini, A. Trovarelli, J. Llorca, G.W. Graham, W.H. Weber, M. Maciejewski, A. Baiker, J. Catal. 194 (2000) 461–478.
[33] E. Rocchini, M. Vicario, J. Llorca, C. de Leitenburg, G. Dolcetti, A. Trovarelli, J. Catal. 211 (2002) 407–421.
[34] H. Vidal, S. Bernal, R.T. Baker, D. Finol, J.A. Perez-Omil, J.M. Pintado, J.M. Rodrıguez-Izquierdo, J. Catal. 183 (1999) 53–62.
[35] G.A.H. Mekhemer, Phys. Chem. Chem. Phys. 4 (2002) 5400–5405.
[36] C. Cannas, M. Casu, M. Mainas, A. Musinu, G. Piccaluga, S. Polizzi, A. Speghini, M. Bettinelli, J. Mater. Chem. 13 (2003) 3079–3084.
[37] S. Duhan, P. Aghamkar, Acta Phys. Pol. A 113 (6) (2008) 1671–1677.
[38] G. Lupina, T. Schroeder, J. Dabrowski, Ch. Wenger, A. Mane, G. Lippert, H.-J. Müssig, P. Hoffmann, D. Schmeisser, Appl. Phys. Lett. 87 (2005) 092901.
[39] G. Bocquillon, C. Chateau, C. Loriers, J. Loriers, J. Solid State Chem. 20 (1977) 135–141.
[40] M.A. Małecka, U. Burkhardt, D. Kaczorowski, M.P. Schmidt, D. Goran, L. Kępiński, J. Nanopart. Res. 11 (2009) 2113–2124.
[41] I. Hartenbach, F. Lissner, T. Schleid, Z. Naturforsch. 58b (2003) 925–927.
[42] T. Yamamoto, T. Matsuyama, T. Tanaka, T. Funabiki, S. Yoshida, J. Mol. Catal. A: Chem. 155 (2000) 43–58.
[43] T. Yamamoto, T. Tanaka, T. Matsuyama, T. Funabiki, S. Yoshida, Solid State Commun. 111 (1999) 137–142.